

Effects of trace La additions on the microstructures and properties of nanoprecipitates strengthened Cu–Zr alloys

Tongmin Wang,^{a)} Mingyu Li, Huijun Kang,^{b)} Wei Wang, Cunlei Zou, and Zongning Chen
Key Laboratory of Materials Modification by Laser, Ion and Electron Beams (Ministry of Education), School of Material Science and Engineering, Dalian University of Technology, Dalian 116024, China

(Received 5 September 2014; accepted 1 December 2014)

The effects of trace La additions on the microstructures and mechanical properties of Cu–0.2 wt% Zr alloy have been investigated. Traditional thermo-mechanical processing was applied to the Cu–Zr alloys. Isochronal aging and isothermal aging were used to optimize the aging conditions. According to the hardness and conductivity tests, the optimized aging condition should be 150 min isothermal holding at 400 °C following 85% cold-rolling. If the as-cast sample is subjected to aging, the addition of La obviously refines the microstructures. After cold-rolling, however, the La addition has no significant effects on the grain size of the aged sample. SEM and TEM are combined to observe the distribution and morphology of the precipitates, which are identified to be Cu₅Zr. The addition of La can improve the hardness and conductivity simultaneously in the as-cast samples after aging, while it improves the hardness and strength and decreases the conductivity slightly in the cold-rolled samples after aging. XRD and TEM results show that the lattice parameter and the dislocation density are increased by the addition of La.

I. INTRODUCTION

Copper-based alloys, due to the combination of good thermal conductivity, high electrical conductivity, and high mechanical strength in engineering applications, have attracted considerable attention over the past few decades.¹ Dissolved solutes in copper can greatly improve the strength of the matrix, but they obviously reduce the electrical conductivity, such as Cu–Ni–Si,² Cu–Fe–Cr,^{3,4} and Cu–Zn⁵ alloys. At present, precipitation hardening is a promising method to realize high strength and electrical conductivity. Alloys using this strategy include Cu–Cr–Zr^{1,6} and Cu–Zr^{7–10} alloys. Cu–Zr alloys are mostly used in miniaturized electronic devices and electric resistance welding electrodes.^{9,11} However, the relatively low strength of the Cu–Zr alloys limits their applications. Therefore, it is important to further improve the mechanical properties of the alloys.

Many attempts have been done to improve the strength of Cu–Zr alloys and preserve their high level of electrical conductivity, and partial successes have been achieved. Arnberg et al.⁷ prepared Cu–0.5 wt% Zr alloys by rapid solidification technology. The alloys were obtained with the tensile strength of 482 MPa and electrical conductivity of 83%IACS after heat treatment. Azimi and Akbari⁸ produced nanostructured Cu–6 wt% Zr alloys by

mechanical alloying and the hardness of the alloy reached 220 HV. In addition, severe plastic deformation has been extensively applied in high strength, high conductivity Cu–Zr alloy. Muramatsu et al.⁹ used a large degree of deformation reductions in the wire-drawing process. Finally, the strength and electrical conductivity of the Cu–0.5 at.% Zr alloy were 690 MPa and 83%IACS without aging process. With eight passes of equal-channel angular pressing (ECAP), the maximum tensile strength of Cu–0.18 wt% Zr reached 506 MPa.¹⁰ It was also reported in other studies that the addition of Cr and Ag can significantly improve the strength without deteriorating the conductivity.¹²

It is well-known that rare earth element, due to the special physical and chemical characteristics, could positively influence the precipitates of the age-hardenable alloys and thus influence the properties. Guo et al.¹³ showed that rare earth element could promote spheroidization and dispersion of the precipitates in Cu–Fe–P–Cr alloys. The addition of rare earth Y in the Al–Zr alloys obviously accelerated the precipitating kinetics of Al₃Zr through the formation of Al₃(Zr,Y) precipitates.¹⁴ Up to now, the content of rare earth is basically higher than 0.03%, but the effects of lower content have remained elusive.

In this paper, the effects of trace La on the Cu–Zr alloy and the aging behavior of Cu–Zr–(La) alloys during the thermo-mechanical treatments were studied. The alloys were treated by feasibly conventional cold-rolling and aging. The tensile strength, hardness, and conductivity were investigated to optimize the aging condition.

Address all correspondence to these authors.

^{a)}e-mail: tmwang@dlut.edu.cn

^{b)}e-mail: kanghuijun@dlut.edu.cn

DOI: 10.1557/jmr.2014.382

II. EXPERIMENTAL

Cu–Zr and Cu–Zr–La alloys were prepared by melting the mixtures of electrolytic copper (99.99 wt%), pure zirconium (99.5 wt%), and rare earth La (99.2 wt%) in a vacuum-induction melting furnace under an argon atmosphere. Casting was carried out in a graphite mold with a size of $\Phi 40 \times 120$ mm. The chemical compositions of the alloy were analyzed by inductively coupled plasma (Table I). After the removal of oxidation layers and surface defects, the billets of $30 \times 30 \times 120$ mm were homogenized at 850 °C for 4 h and subsequently hot-rolled to a thickness of 15 mm. The rolled samples were then solution-treated at 960 °C for 1 h followed by water-quenching. The solution-treated plates were planned on both sides to remove oxidation layers and cold-rolled with 80 or 85% reduction at ambient temperature, respectively. These plates thus obtained were cut into small pieces with designed sizes for aging treatment. The isochronal aging at 300–500 °C for 60 min and isothermal aging at 400 °C for 30–180 min were carried out in a tubular electric resistance furnace with a temperature accuracy of ± 1 °C.

The microstructures of the aging cast and aging rolled samples (aging cast and aging rolled represent those as-cast and rolled specimens that were subjected to aging) were investigated by an optical microscope and a scanning electron microscope (SEM, JSM-5600LV, JEOL Company, Tokyo, Japan). The samples were mechanically ground, polished, and etched with a solution of FeCl_3 , HCl, and absolute alcohol mixture. The number and distribution of the particles were quantified by image analysis of the SEM micrographs. The total number of particles used for this analysis was no less than 300 for each experiment and the particle number density was measured in the area of $1 \mu\text{m} \times 1 \mu\text{m}$ at 6 SEM images. For TEM samples, the discs of 3 mm in diameter punched from aged plates were ground to 60–80 μm and then double jet thinned using a 25% nitric acid in methanol solution at about -30 °C. TEM observations were carried out by a transmission electron microscope (TEM) operating at 200 kV (JEM-2100). X-ray diffraction (XRD) was conducted on EMPYREAN equipped with a Cu radiation target.

Vickers hardness (HV) was measured on a MH-50 type microhardness tester using a load of 100 gf and a dwell time of 10 s. Before the measurement, standard

specimens were used to correct the hardness. Samples with a length of 30 mm were tensile-tested on a CSS-2205 tensile machine with a strain rate of 2 mm/min at 298 K. Electrical resistance was measured by a D60K digital electrical instrument.

III. RESULTS AND DISCUSSION

A. Microstructures and properties of the aging cast specimen

Figures 1(a) and 1(b) show the microstructures of the aging cast Cu–Zr and Cu–Zr–La alloys. The specimens were aged at 550 °C for 120 min. The addition of La obviously refines the microstructures of the alloy and the morphologies of the Cu solid solution are modified from a large columnar crystal to fine equiaxed grains.

Figure 2(a) shows the microstructures in the vicinity of grain boundary of the Cu–Zr–La alloy. Club-shaped and oval-shaped particles are observed at the grain boundaries and high fractions of nanosized dots (33.7 nm) are homogeneously distributed in the matrix [Figs. 2(a) and 2(b)]. TEM results [Fig. 3(a)] reveal that the mean size of precipitates is 26.42 nm, thus it can be deduced that the dots in the SEM micrographs are Zr-rich precipitates considering the similar size, shape, and distribution.^{15,16} Compared to the TEM, the SEM image has a wider field view and reveals a larger number of precipitates. The morphology and spatial distribution in the SEM image are more reliable and clear. To better observe the smaller particles, high-resolution TEM images are shown in Figs. 3(b) and 3(c). Fine precipitates with lobe-lobe contrast are found in Fig. 3(b) (marked by rectangles) and they display spot-shape or extend regions, which exhibits well-defined alternate bright and dark parallel Moiré patterns.^{6,17} The mean spacing D in Moiré patterns is ~ 1.2 nm. Meanwhile, the precipitates with sizes of 2–5 nm show apparent dark contrast (marked by dotted circles). The single spherical precipitation (3.3 nm) is coherent with the matrix as shown in the inset of Fig. 3(c). The selected area electron diffraction with a zone axis of $[1-10]_{\text{Cu}}$ in Fig. 3(d) exhibits two sets of reflections. One is from the matrix and the other from the precipitates. The streaking seen in the pattern reveals that the precipitates have an ordered fcc structure and the value of d is consistent with all the interplanar spacing of the Cu_5Zr phase. There is a controversy about the composition of Zr-containing precipitates (Cu_3Zr , Cu_4Zr , $\text{Cu}_{51}\text{Zr}_{14}$, or Cu_5Zr). Recently, several studies on Cu–Zr alloys have identified Cu_5Zr as the Zr-containing precipitate phase^{7,18–20} which is also evidenced by the above results in this paper. The Cu_5Zr peaks are also found in the XRD spectrum (Fig. 4), which further confirms the dominance of this phase. But the effects of trace La on the morphology and spatial distribution of the precipitates are less evident.

TABLE I. Chemical composition of the Cu–Zr and Cu–Zr–La alloys.

Alloy	Analyzed composition (wt%)		
	Zr	La	Cu
Cu–Zr	0.206	...	Bal.
Cu–Zr–La	0.1906	0.0058	Bal.

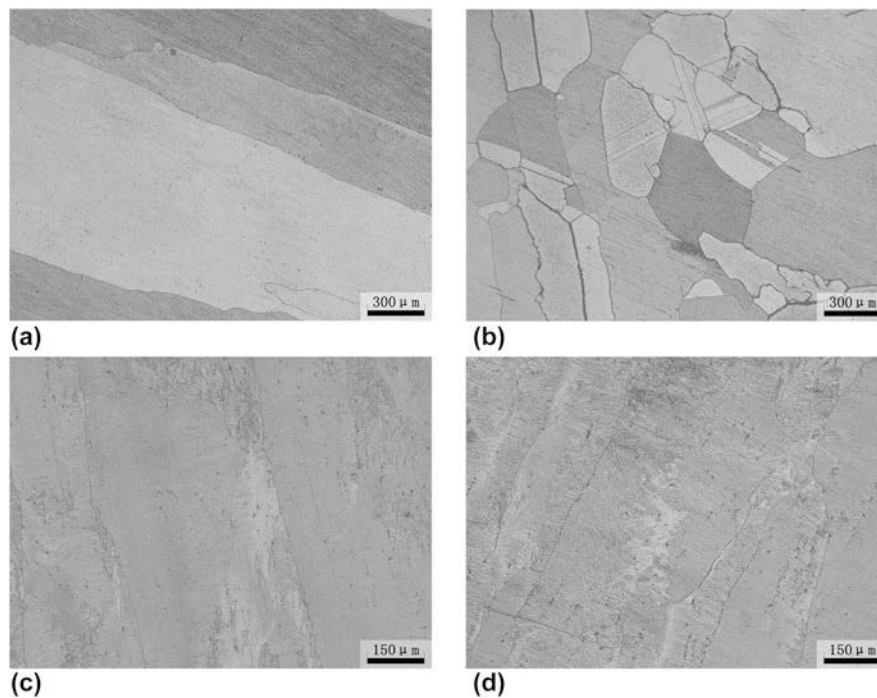


FIG. 1. Optical micrograph of the Cu–Zr–(La) alloys: aging cast (a) Cu–Zr and (b) Cu–Zr–La alloys aged at 550 °C for 2 h; aging rolled (c) Cu–Zr and (d) Cu–Zr–La alloys aged at 400 °C for 150 min.

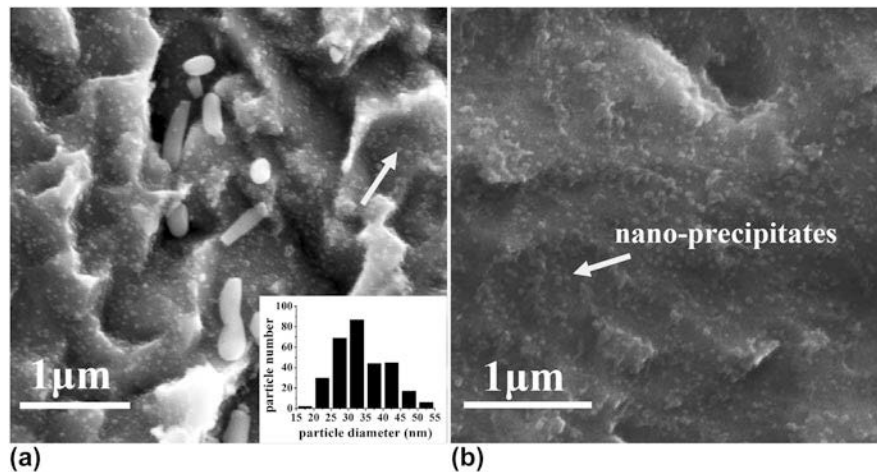


FIG. 2. SEM micrographs of (a) the vicinity of grain boundary and (b) the interior of the grains of the aging cast Cu–Zr–La alloy aged at 550 °C for 2 h.

The electrical conductivity and hardness are improved simultaneously (from 96%IACS, 91.86 HV to 96.9% IACS, 94.44 HV) by the addition of La under the condition of aging cast. These improvements can be ascribed to the following two aspects. On the one hand, the addition of La could react preferentially with the impurities such as O, H, S, Pb, Te, and Bi and finally form high melting point and stable compounds at elevated temperature. These compounds are easily removed because of their lower densities.¹³ Therefore, the purification of the melt can effectively improve the

strength and electrical conductivity. On the other hand, compared to the Cu–Zr alloy, the grains in the Cu–Zr–La alloy are finer. According to the Hall–Petch relationship, the finer the grain of the alloy is, the higher the strength of the alloy will be. The hardness of the Cu–Zr–La alloy is thus slightly higher than that of the Cu–Zr alloy. It also indicates that the diffusion distance of Zr atoms during the solution process is shortened, leading to a more uniform distribution of Zr atoms in the grains. Finally, finer and more uniformly distributed precipitates are formed in the grains during the aging process.²¹

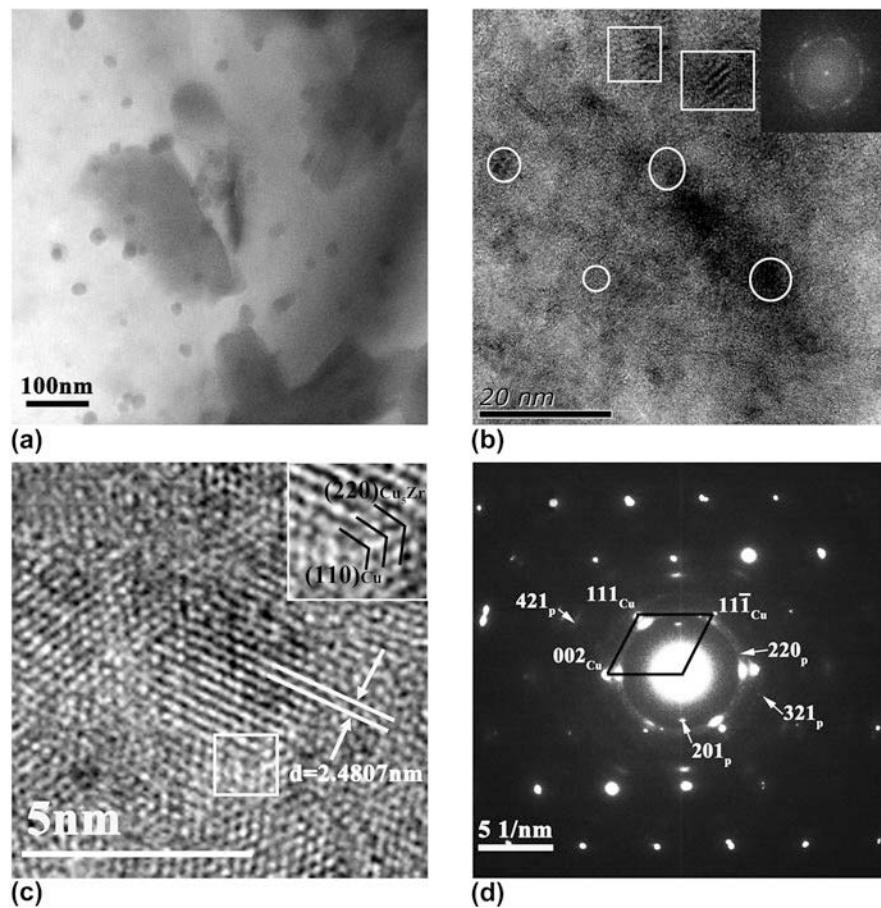


FIG. 3. (a, b) Bright field TEM micrographs of the aging cast Cu–Zr–La alloy; (c) high-resolution TEM image of precipitates; and (d) the corresponding SAED patterns (p-precipitate), zone axis close to $[1-1\ 0]_{Cu}$.

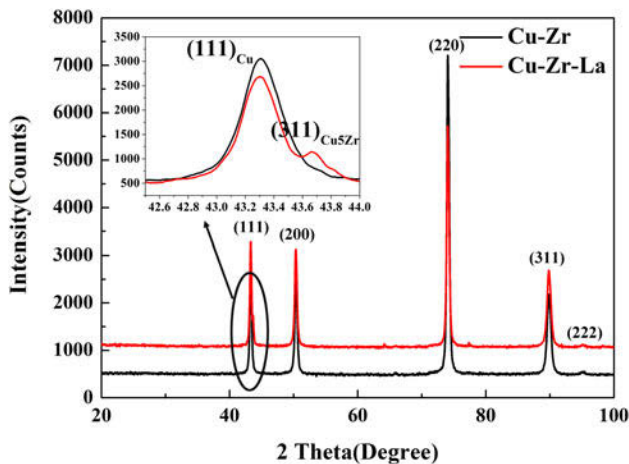


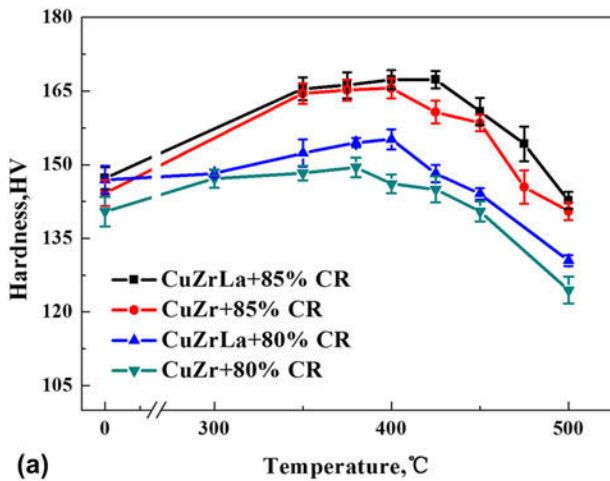
FIG. 4. Diffraction peaks for Cu–Zr–(La) alloys. The inset shows the position of the angle diffraction peaks about 43° .

B. Effects of aging temperature and time on hardness and conductivity of the alloys after cold-rolling

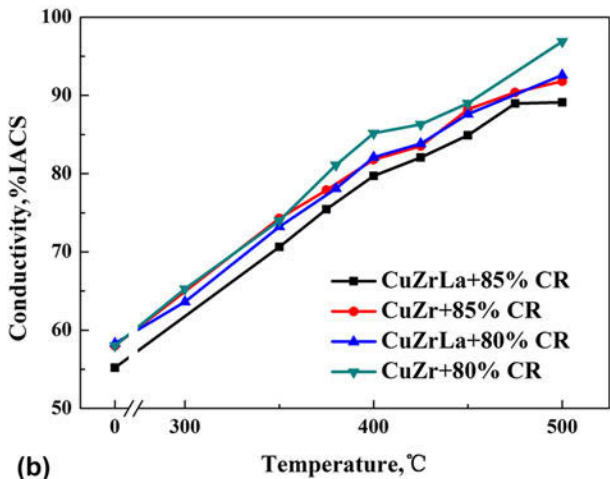
Cold-rolled samples were aged for 60 min at different temperatures to optimize the aging temperature for

Cu–Zr–(La) alloys. Figure 5 shows the hardness and electrical conductivity of Cu–Zr–(La) alloys as a function of temperature during isochronal aging for 60 min. All the alloys have large hardening responses from 300 to 500 °C and attain the peak microhardness when aging at 400 °C. The peak values after 85% cold-rolling are 165.56 and 167.32 HV, while the peak values after 80% cold-rolling are 146.08 and 156.15 HV, respectively. The conductivity of these alloys continues to increase in the entire temperature range, which can be ascribed to the high precipitating kinetics and recrystallization of the alloys.¹

Hardness and conductivity curves of 400 °C isothermal aged Cu–Zr–(La) alloys are shown in Fig. 6. At the initial stage of the aging, the hardness increases rapidly and reaches the peak after aging for 150 min. Then the hardness begins to decline. The conductivity increases dramatically to the peak at first and maintains approximately a stable value with further aging. At the beginning of the isothermal aging, Cu₅Zr particles precipitate rapidly out of the supersaturated alloy matrix, therefore a steep increase in the conductivity occurs owing to the high decomposition kinetics. As the aging time increases, the



(a)



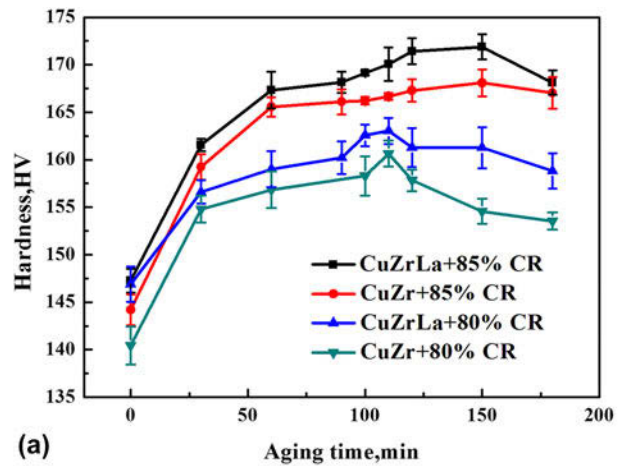
(b)

FIG. 5. Vickers microhardness and electrical conductivity evolution of the Cu–Zr and Cu–Zr–La alloys during isochronal aging for 1 h.

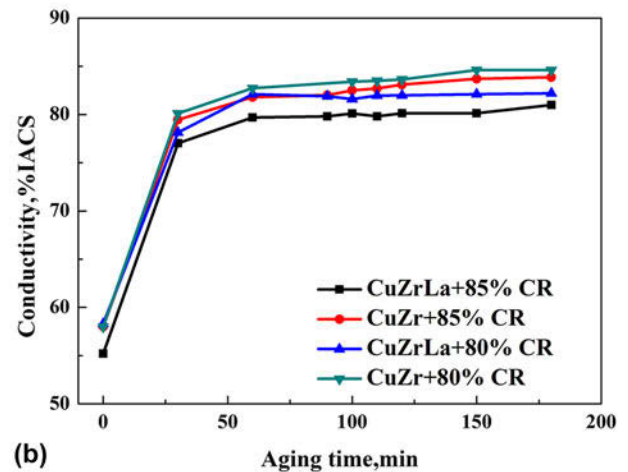
solute concentration approaches equilibrium and the electrical conductivity increases marginally.

It is interesting to note that the hardness of 85% cold-rolled Cu–Zr–(La) alloys is ~10 HV higher than that of 80% cold-rolled alloys, while the conductivity is ~2% IACS lower at the same aging treatment process. Cold-rolling has little influence on the conductivity, but it can greatly enhance the hardness. Thus, the reduction of 85% can be considered as the suitable deformation reduction for the Cu–Zr–(La) alloys. However, this trend of the conductivity with the increase of deformation reduction does not agree with Refs. 22 and 23. Such a discrepancy may be caused by the manufacturing process. Once 80% cold-rolling reaches, cold deformation is so difficult that prolonged duration of the rolling process is necessary. In this process, the dislocation density increases significantly and then the conductivity will be reduced.

The peak hardness and the corresponding conductivity of the 85% cold-rolled Cu–Zr and Cu–Zr–La alloys aged



(a)



(b)

FIG. 6. Hardness and electrical conductivity of the Cu–Zr and Cu–Zr–La alloys as a function of aging time during isothermal aging at 400 °C.

at 400 °C for 150 min are 168.08 HV, 83.7%IACS and 173.04 HV, 80.1%IACS, respectively. This aging condition is recognized as the peak-aged state. It is worth noting that the hardness of the alloys with the addition of La can be improved by ~5 HV and the conductivity decreases by 2–3%IACS. This effect contradicts with that in the case of aging cast and the reason will be discussed in detail later.

C. Microstructures and properties of the aging rolled specimens

Figures 1(c) and 1(d) show the optical microstructures of the Cu–Zr and Cu–Zr–La alloys aged for 150 min at 400 °C. The cold deformed structure with markedly elongated grains aligned along the rolling direction is observed and the grain size of the alloys reveals no significant difference. Figure 7 shows the precipitates in the Cu–Zr–La alloy aged for 150 min at 400 °C. The mean size of the precipitates is 14.5 nm and the number

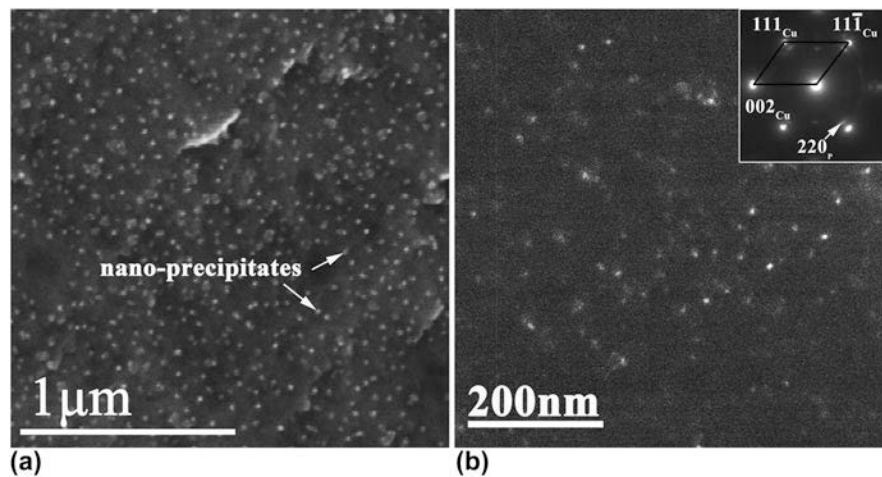


FIG. 7. (a) SEM image of the 85% cold-rolled Cu–Zr–La alloy aged at 400 °C for 150 min and (b) dark field image and selected electron diffraction pattern of the alloys (p-precipitate), zone axis close to $[1-1 0]_{\text{Cu}}$.

density is $1.67 \times 10^{12} \text{ m}^{-2}$. Figure 8(a) reveals the distribution of the precipitates in the Cu–Zr–La alloy aged for 90 min at 425 °C. Coarsening of the precipitates has occurred locally. The maximum and mean sizes of the precipitates are 41.5 and 21.6 nm, respectively. Figure 8(c) shows that the nanoparticles assemble into a larger particle by the oriented attachment mechanism.²⁴ From the consistent results in the SEM [Fig. 8(a)] and TEM [Figs. 8(b) and 8(c)] observations, we can conclude that the alloy is at over-aging state. Besides ~ 20 nm precipitates, there also exists near-spherical Zr-rich precipitates with a mean size of ~ 4 nm [Fig. 8(d)].

Table II shows the properties of the Cu–Zr and Cu–Zr–La alloys under different thermo-mechanical processing conditions. When aged for 150 min at 400 °C, the ultimate tensile strength (σ_{UTS}) and yield strength ($\sigma_{0.2}$) of the Cu–Zr–La alloy attain the maximum values as 530 and 492 MPa, respectively, and the corresponding conductivity still keeps the level of 80%IACS. However, σ_{UTS} and $\sigma_{0.2}$ of the Cu–Zr alloy are 507 and 459 MPa. Under the same aging conditions, the strength of Cu–Zr–La alloy is higher than that of Cu–Zr alloy, but the conductivity is lower. These variations of σ_{UTS} and $\sigma_{0.2}$ are consistent with the trend in Vickers hardness plotted in Figs. 5 and 6. In addition, the σ_{UTS} and $\sigma_{0.2}$ of the alloy aged for 150 min at 400 °C are higher than those aged for 120 min at 400 °C.

The higher strength of the alloys aged for 150 min at 400 °C with respect to that aged for 90 min at 425 °C confirms that aging for a long time at lower temperatures is an effective method to attain the better properties. At lower temperatures, the atomic diffusion of the solute atoms is slow and the precipitates are not susceptible to aggregate and grow. However, this process will take a long time to achieve the full precipitation state. Moreover, the density of the precipitates aged at lower temperatures is higher due to the different supersaturation

degrees in the Cu–Zr phase diagram.^{22,25} The strengthening mechanism of the alloys can be described by the Orowan–Ashby equation.¹⁸

$$\tau_{\text{OA}} = 0.84 \frac{Gb}{2\pi(1-\nu)^{1/2}\lambda} \ln\left(\frac{\pi r}{2r_0}\right)$$

Here, τ_{OA} is the critical resolved shear stress, r is the average radius of the Cu_5Zr particle, r_0 is the inner cut-off radius of the dislocation, and λ is the spacing between particles in the glide plane beyond the peak strength. The greater the average radius of the Cu_5Zr particle is, the lower the increase of the critical resolved shear stress will be. The size of the precipitates in the alloy aged at 425 °C is 21.6 nm, while the size is 14.5 nm at the peak-aged state. Thus, the strength of the alloys aged for 90 min at 425 °C is lower than that aged for 150 min at 400 °C.

D. Analysis of the effects of La in the aging rolled samples

The effects of trace La on the alloys in the aging rolled state were divided into three points to discuss: purification, distortion of lattice, and dislocation density.

Compared to the aging cast alloys, the grain sizes between the aging rolled alloys are of no significant difference. Grain refinement has not been retained in aging rolled state, but the purification effect still influences the alloy. Purification will improve the strength and the electrical conductivity as described in Sec. III. A.

The atomic radius of Cu is $R_{\text{Cu}} = 0.128$ nm, while the atomic radii of Zr and La are $R_{\text{Zr}} = 0.159$ nm²⁶ and $R_{\text{La}} = 0.195$ nm, respectively. When the larger Zr and La atoms dissolve into the Cu matrices, the lattice parameter of Cu will increase due to lattice distortion. At a peak-aged state, the lattice parameter of Cu–Zr alloy is calculated to be 3.61744 ± 0.000537 nm from the

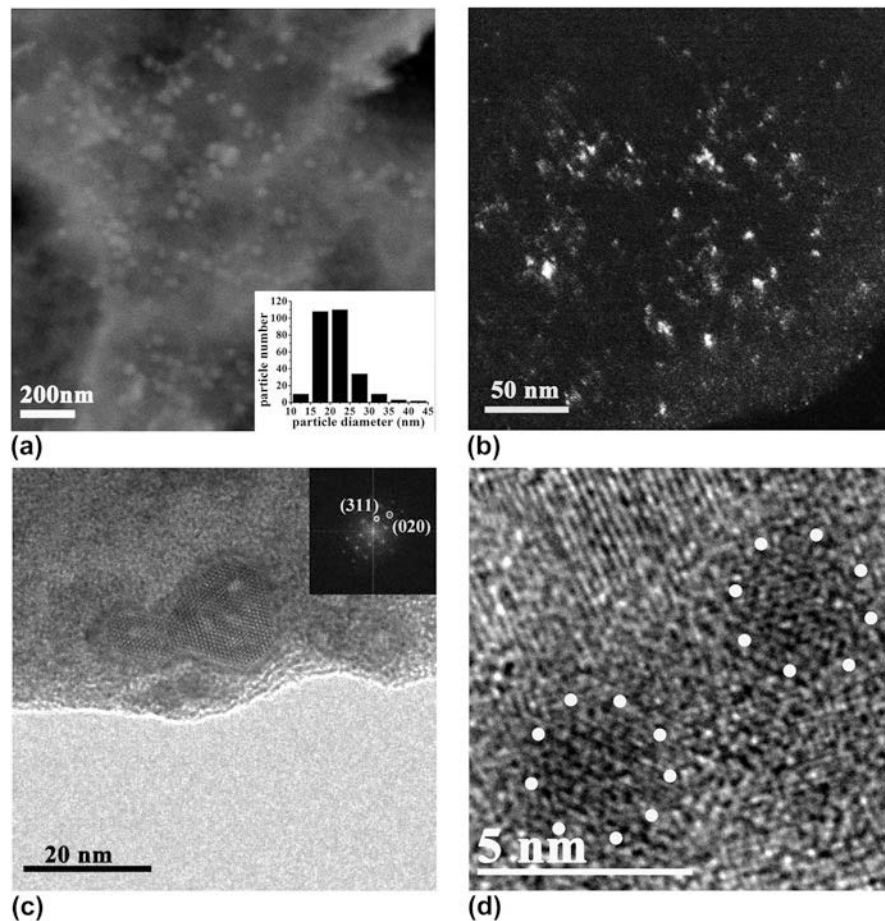


FIG. 8. (a) SEM and (c) bright field images of the 85% cold-rolled Cu–Zr–La alloy aged at 425 °C for 90 min, the corresponding FFT spectra of the precipitation in the inset which indicates that the precipitation is the Cu_5Zr phase; (b) dark field image of the Cu–Zr–La alloy; and (d) high-resolution TEM image of precipitates.

TABLE II. Properties of 85% cold-rolled Cu–Zr and Cu–Zr–La alloys under different thermo-mechanical processing conditions.

Alloy	Condition	Hardness	$\sigma_{0.2}$ (MPa)	σ_{UTS} (MPa)	Cond. (%IACS)	δ (%)
Cu–Zr	Age 120 min 400 °C	167.28	438	503	83.1	16
	Age 150 min 400 °C	168.08	459	507	83.7	15
	Age 90 min 425 °C	161.02	430	472	84	16
Cu–Zr–La	Age 120 min 400 °C	171.42	482	522	80.1	16
	Age 150 min 400 °C	173.04	492	530	80.1	12.5
	Age 90 min 425 °C	170.36	476	515	82.1	17.5

XRD peaks (Fig. 4), while that of Cu–Zr–La alloy is 3.6186 ± 0.000418 nm. Both of two parameters are bigger than that of pure Cu (3.615 nm) and the deviation is very small due to the extremely low solubility of Zr and La in Cu matrices at room temperature. Furthermore, the more deviation of the lattice parameter in Cu–Zr–La alloy leads to the lower electrical conductivity.²⁷ Meanwhile, the lattice distortion caused by solute atoms can form long-term stress field, and the dislocation must overcome the stress field to slip in the matrix. This process improves the strength and decreases the plasticity, which can be confirmed from Table II.

It is observed that high density of dislocations is introduced by the cold-rolling as shown in Fig. 9. The dislocations can form preferred nucleation sites for precipitates and easily become diffusion paths for dissolved solute atoms, while the adverse effect is that they also scatter conducting electrons, leading to a decrease in conductivity.¹ The dislocation densities in the matrices of the Cu–Zr and Cu–Zr–La alloys in a peak-aged state are estimated from their XRD peak broadenings as $0.607 \times 10^{14} \text{ m}^{-2}$ and $1.105 \times 10^{14} \text{ m}^{-2}$, respectively.²⁸ As is known, if the grains are smaller than 100 nm, the grain size will affect the peak broadening. The grain sizes

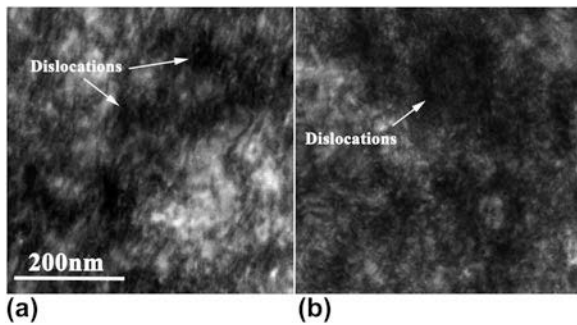


FIG. 9. Dislocation morphologies of the (a) Cu–Zr and (b) Cu–Zr–La alloys aged for 150 min at 400 °C after 85% cold-rolling.

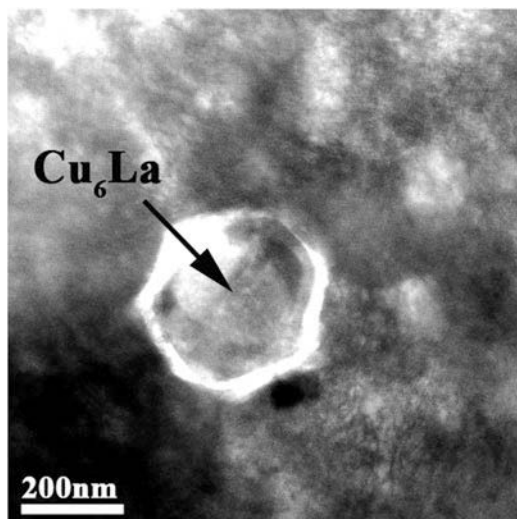


FIG. 10. The bright field image of the Cu_6La phase in the Cu–Zr–La alloy.

of the studied alloys are far more than 100 nm, so the marked broadening in the Cu peak is caused by the variation of dislocation density.²⁹ Due to the tiny solid solubility of La in Cu, the intermetallic Cu_6La phase is facile to form through the fluctuations of structure, composition, and energy, as shown in Fig. 10. The composition of this phase, measured by energy dispersive spectrometer (EDS) equipped in TEM, is identified as 84.58 at.% Cu and 15.42 at.% La. The formation of the Cu_6La phase effectively impedes the dislocation sliding and the dislocations are easily accumulated in the vicinity of the particles, which prevent the dislocations to annihilate in the grain boundary. The dislocations can also impact the hardness and ultimate tensile strength. The strength increment due to dislocation strengthening $\Delta\sigma_d$ is:³⁰

$$\Delta\sigma_d = M\alpha Gb\rho^{1/2},$$

where ρ is the dislocation density, α is a constant, which for fcc metals is ~ 0.2 , $M = 3.06$ is the mean orientation factor for the fcc matrix, G is the shear modulus of the

matrix, 41.0 GPa, and b is the Burgers vector of the matrix. Therefore, increasing the dislocation density will improve the hardness and ultimate tensile strength of the alloy.

IV. CONCLUSIONS

According to the results obtained in this work, the following conclusions can be drawn:

(1) In aging cast, the addition of trace La obviously refines the grain structures of Cu–Zr alloys. After cold-rolling and aging processes, the addition of trace La improves the strength significantly, but decreases the conductivity slightly. The purification, distortion of lattice, and dislocation density are considered to be responsible for these effects.

(2) Aging for longer time at lower temperatures is an effective method to attain the peak-aged state. The Zr-containing precipitation is Cu_5Zr , the crystal structure of which is face-centered cubic and coherent with the Cu matrix.

(3) The ultimate tensile strength and conductivity of the Cu–Zr–La alloy reach 530 MPa and 80.1% IACS, respectively, after 85% cold-rolling and aging for 150 min at 400 °C.

ACKNOWLEDGMENTS

The authors gratefully acknowledge the supports of National Natural Science Foundation of China (Nos. 51274054, U1332115, 51271042, 51375070, 51401044), the Key Grant Project of Chinese Ministry of Education (No. 313011), the Science and Technology Planning Project of Dalian (No. 2013A16GX110), the China Postdoctoral Science Foundation (2014M551075), and the Fundamental Research Funds for the Central Universities.

REFERENCES

1. C. Xia, W. Zhang, Z. Kang, Y. Jia, Y. Wu, R. Zhang, G. Xu, and M. Wang: High strength and high electrical conductivity Cu–Cr system alloys manufactured by hot rolling–quenching process and thermomechanical treatments. *Mater. Sci. Eng., A* **538**, 295 (2012).
2. Z. Li, Z.Y. Pan, Y.Y. Zhao, Z. Xiao, and M.P. Wang: Microstructure and properties of high-conductivity, super-high-strength Cu–8.0Ni–1.8Si–0.6Sn–0.15Mg alloy. *J. Mater. Res.* **24**, 2123 (2013).
3. H. Fernee, J. Nairn, and A. Atrens: Precipitation hardening of Cu–Fe–Cr alloys, part I mechanical and electrical properties. *J. Mater. Sci.* **36**, 2711 (2001).
4. H. Fernee, J. Nairn, and A. Atrens: Precipitation hardening of Cu–Fe–Cr alloys, part II microstructural characterisation. *J. Mater. Sci.* **36**, 2721 (2001).
5. Y.H. Zhao, X.Z. Liao, Z. Horita, T.G. Langdon, and Y.T. Zhu: Determining the optimal stacking fault energy for achieving high ductility in ultrafine-grained Cu–Zn alloys. *Mater. Sci. Eng., A* **493**, 123 (2008).

6. H.T. Zhou, J.W. Zhong, X. Zhou, Z.K. Zhao, and Q.B. Li: Microstructure and properties of Cu-1.0Cr-0.2Zr-0.03Fe alloy. *Mater. Sci. Eng., A* **498**, 225 (2008).
7. L. Arnberg, U. Backmark, N. Bäckström, and J. Lange: A new high strength, high conductivity Cu-0.5wt.% Zr alloy produced by rapid solidification technology. *Mater. Sci. Eng.* **83**, 115 (1986).
8. M. Azimi and G.H. Akbari: Characterization of nano-structured Cu-6wt.% Zr alloy produced by mechanical alloying and annealing methods. *J. Alloys Compd.* **555**, 112 (2013).
9. N. Muramatsu, H. Kimura, and A. Inoue: Microstructures and mechanical properties of highly electrically conductive Cu-0.5, Cu-1 and Cu-2 at% Zr alloy wires. *Mater. Trans.* **54**, 176 (2013).
10. R. Kužel, M. Janeček, Z. Matěj, J. Čížek, M. Dopita, and O. Srba: Microstructure of equal-channel angular pressed Cu and Cu-Zr samples studied by different methods. *Metall. Mater. Trans. A* **41**, 1174 (2009).
11. D.E. Tyler and W.T. Black: *ASM Handbook*, 10th ed. (ASM International Press, Detroit, The United States of America, 1990), p. 770. Olin Corporation.
12. V.K. Sarin and N.J. Grant: Cu-Zr and Cu-Zr-Cr alloys produced from rapidly quenched powders. *Metall. Trans.* **3**, 875 (1972).
13. F.A. Guo, C.J. Xiang, C.X. Yang, X.M. Cao, S.G. Mu, and Y.Q. Tang: Study of rare earth elements on the physical and mechanical properties of a Cu-Fe-P-Cr alloy. *Mater. Sci. Eng., B* **147**, 1 (2008).
14. Y. Zhang, H. Gao, Y. Kuai, Y. Han, J. Wang, B. Sun, S. Gu, and W. You: Effects of Y additions on the precipitation and recrystallization of Al-Zr alloys. *Mater. Charact.* **86**, 1 (2013).
15. J. Lin and L. Meng: Effect of aging treatment on microstructure and mechanical properties of Cu-Ag alloys. *J. Alloys Compd.* **454**, 150 (2008).
16. F. Bittner, S. Yin, A. Kauffmann, J. Freudenberger, H. Klauß, G. Korpala, R. Kawalla, W. Schillinger, and L. Schultz: Dynamic recrystallisation and precipitation behaviour of high strength and highly conducting Cu-Ag-Zr alloys. *Mater. Sci. Eng., A* **597**, 139 (2014).
17. T. Fujii, H. Nakazawa, M. Kato, and U. Dahmen: Crystallography and morphology of nanosized Cr particles in a Cu-0.2% Cr alloy. *Acta Mater.* **48**, 1033 (2000).
18. S.G. Jia, X.M. Ning, P. Liu, M.S. Zheng, and G.S. Zhou: Age hardening characteristics of Cu-Ag-Zr alloy. *Met. Mater. Int.* **15**, 555 (2009).
19. M.Y.-W. Lou and N.J. Grant: Identification of Cu₅Zr phase in Cu-Zr alloys. *Metall. Trans. A* **15**, 1491 (1984).
20. J. Ružić, J. Stašić, V. Rajković, and D. Božić: Synthesis, microstructure and mechanical properties of ZrB₂ nano and microparticle reinforced copper matrix composite by in situ processings. *Mater. Des.* **62**, 409 (2014).
21. D. Zhou, F. Qiu, and Q. Jiang: Simultaneously increasing the strength and ductility of nano-sized TiN particle reinforced Al-Cu matrix composites. *Mater. Sci. Eng., A* **596**, 98 (2014).
22. C. Xia, Y. Jia, W. Zhang, K. Zhang, Q. Dong, G. Xu, and M. Wang: Study of deformation and aging behaviors of a hot rolled-quenched Cu-Cr-Zr-Mg-Si alloy during thermomechanical treatments. *Mater. Des.* **39**, 404 (2012).
23. X. Zhang, J. Han, L. Chen, B. Zhou, Y. Xue, and F. Jia: Effects of B and Y additions on the microstructure and properties of Cu-Mg-Te alloys. *J. Mater. Res.* **28**, 2747 (2013).
24. J. Zhang, F. Huang, and Z. Lin: Progress of nanocrystalline growth kinetics based on oriented attachment. *Nanoscale* **2**, 18 (2010).
25. D. Arlas and J.P. Ablata: Cu-Zr (copper-zirconium). *Bull. Alloy Phase Diagrams* **11**, 452 (1990).
26. A. Gaganov, J. Freudenberger, E. Botcharova, and L. Schultz: Effect of Zr additions on the microstructure, and the mechanical and electrical properties of Cu-7 wt.% Ag alloys. *Mater. Sci. Eng., A* **437**, 313 (2006).
27. Q. Liu, X. Zhang, Y. Ge, J. Wang, and J.Z. Cui: Effect of processing and heat treatment on behavior of Cu-Cr-Zr alloys to railway contact wire. *Metall. Mater. Trans. A* **37**, 3233 (2006).
28. Y.H. Zhao, X.Z. Liao, Z. Jin, R.Z. Valiev, and Y.T. Zhu: Microstructures and mechanical properties of ultrafine grained 7075 Al alloy processed by ECAP and their evolutions during annealing. *Acta Mater.* **52**, 4589 (2004).
29. Y.H. Zhao, J.F. Bingert, X.Z. Liao, B.Z. Cui, K. Han, A.V. Sergueeva, A.K. Mukherjee, R.Z. Valiev, T.G. Langdon, and Y.T. Zhu: Simultaneously increasing the ductility and strength of ultra-fine grained pure copper. *Adv. Mater.* **18**, 2949 (2006).
30. H. Wen, T.D. Topping, D. Isheim, D.N. Seidman, and E.J. Lavermia: Strengthening mechanisms in a high-strength bulk nanostructured Cu-Zn-Al alloy processed via cryomilling and spark plasma sintering. *Acta Mater.* **61**, 2769 (2013).